Cooperative diagnostics for combinations of large-volume metrology systems

Cooperative diagnostics for combinations of large-volume metrology systems

Domenico Maisano[1] and Luca Mastrogiacomo[2]

[1] *domenico.maisano@polito.it* [2] *luca.mastrogiacomo@polito.it*

Politecnico di Torino, DIGEP (Department of Management and Production Engineering), Corso Duca degli Abruzzi 24, 10129, Torino (Italy)

Abstract

Recent studies show that the combined use of Large-Volume Metrology (LVM) systems (e.g., laser trackers, rotary-laser automatic theodolites, photogrammetric systems, etc.) can lead to a systematic reduction in measurement uncertainty and a better exploitation of the available equipment.

The objective of this paper is to present some diagnostic tests for combinations of LVM systems that are equipped with distance and/or angular sensors. Two are the tests presented: a *global* test to detect the presence of potential anomalies during measurement and a *local* test to isolate any faulty sensor(s). This diagnostics is based on the *cooperation* of sensors of different nature, which merge their local measurement data, and it can be implemented in real-time, without interrupting or slowing down the measurement process. The description of the tests is supported by several experimental examples.

Keywords: Large-volume metrology, Distributed sensors, Multi-system combination, Cooperative diagnostics, Statistical test, Measurement consistency.

1. Introduction

The field of *Large-Volume Metrology* (LVM) deals with objects with linear dimensions ranging from several meters to tens of meters (Estler et al., 2002; Peggs et al., 2009; Franceschini et al., 2011; Schmitt et al., 2016). Typical industrial applications concern dimensional verification and assembly of large-sized mechanical components, in which levels of uncertainty of several tenths of millimetre are generally tolerated (Maropoulos et al., 2014; Chen et al., 2015). These applications are typically performed using technologically advanced LVM systems, which are very

expensive and may require time consuming set-up and measurement operations (Franceschini and Maisano, 2014).

LVM systems are usually equipped with *sensors* able to perform local measurements of distances and/or angles. Depending on the sensor layout, LVM systems can be classified into: (i) *centralized*, if sensors are grouped into a unique stand-alone unit (e.g., a laser tracker), or (ii) *distributed*, if sensors are spread around the measurement volume (e.g., a set of rotary-laser automatic theodolites (Maisano et al., 2008)). Even though the existing measuring systems may differ in technology and metrological characteristics, two common features are: (i) the use of some *targets* to be localized, which are generally mounted on a hand-held probe for localizing the points of interest or in direct contact with the measured object's surface, and (ii) the fact that target localization is performed using local measurements by sensors.

For distributed LVM systems, sensors are arranged around the measured object and there are three possible approaches for target localization (Franceschini et al., 2011):

- *Multilateration*, using the *distances* between targets and sensors;
- *Multiangulation*, using the *angles* subtended by targets with respect to sensors;
- *Hybrid techniques*, which are based on the combined use of angles and distances between targets and sensors.

Although several types of LVM systems are (not rarely) available in the same industrial workshop or metrology laboratory, they are often used independently of each other (e.g., a laser tracker is used for certain tasks, a photogrammetric system for others, and so on). This is a rather myopic view because it ignores the benefits that may result from the combination of multiple systems, including but not limited to:

- overcoming the limitations of the individual systems;
- improving measurement accuracy and coverage;
- reducing the risk of measurement errors, due to measurement redundancy.

Franceschini et al. (2016) recently proposed a novel approach, in which a combination of LVM systems that are equipped with sensors of different nature – i.e., sensors with different metrological characteristics and able to measure distances and/or angles –

share their measurement data and cooperate for determining a unique localization of the target. In other words, data provided by a number of sensors from different LVM systems are fused together in order to localize the target (Galetto et al., 2015; Franceschini et al., 2016; Maisano and Mastrogiacomo, 2016). According to this philosophy, the set of (centralized and/or distributed) LVM systems that are used in conjunction can be seen as a single distributed LVM "macro-system", consisting of sensors of different nature.

The purpose of this article is to present some statistical tests, which provide a practical on-line diagnostics functionality. These tests allow to detect possible measurement anomalies and, subsequently, isolate any potentially faulty sensor(s). This diagnostics can be classified as *cooperative*, since it is based on the cooperation of sensors of different nature.

In detail, two statistical tests will be discussed:

- a *global* test, aimed at evaluating the consistency of the target localization, based on the variability of the local measurements by sensors.
- a *local* test that – when a target localization is not considered consistent by the global test – identifies the potentially faulty sensor(s) and (temporarily) excludes them from the target-localization process, without interrupting it.

These tests can interpreted as a generalization of similar tests that have been previously developed: i.e., (i) some tests for distributed LVM systems with distance sensors only and (ii) other tests for distributed LVM systems with angular sensors only; in this sense, this research represents an important update of (Franceschini et al., 2009; Franceschini et al., 2014).

The remainder of this paper is structured into four sections. Section 2 provides some background information, which is helpful to grasp the subsequent description of statistical tests, precisely: (i) basic concepts concerning diagnostics and (ii) a synthetic description of the target-localization mathematical model in use. Section 3 provides a detailed description of the statistical tests, with several experimental examples. Section 4 summarizes the original contributions of this research, focusing on its

implications, limitations and possible future developments. Details on the mathematical model for target localization are contained in the appendix.

2. Background information

2.1 Basic concepts concerning diagnostics

In general, the concept of *consistency of a measurement* is defined as follows. For each measurable quantity *x*, we can define a confidence interval [*LL*, *UL*] (where *LL* stands for Lower Limit and *UL* for Upper Limit). The measure ($\hat{x}$) of the quantity *x* is considered consistent if $\hat{x} \in [LL, UL]$ (Gertler, 1998; Franceschini et al., 2011).

The type-I and -II probability errors (misclassification rates) respectively correspond to:

$$\begin{aligned} \alpha &= \Pr\{\hat{x} \notin [LL, UL] \mid \text{absence of systematic error sources}\} \\ \beta &= \Pr\{\hat{x} \in [LL, UL] \mid \text{presence of systematic error sources}\} \end{aligned}. \quad (1)$$

Usually, *LL* and *UL* reflect the natural variability of the measurement system (which is related to the metrological characteristics of *accuracy*, *reproducibility*, *repeatability*, etc.), in the absence of systematic error sources[1] (JCGM 200:2008, 2008).

For distributed systems, local anomalies in one or more sensors can distort or even compromise the target localization. On the other hand, when these anomalies are recognised, the target-localization results can be corrected by (temporarily) excluding malfunctioning sensor(s). This is the reason why distributed systems are – to some extent – rather "vulnerable" but can be successfully protected by appropriate diagnostic tools.

The diagnostics presented in this paper can be classified as *cooperative*, since the sensor local measurements are used in conjunction: not only for localizing the target but also for detecting possible measurement anomalies/accidents in this process. As mentioned in Sect. 1, this diagnostics includes two tests (global and local), aimed

[1] The authors are aware that systematic measurement errors can never be eradicated completely; this assumption is therefore not valid in general, even though could be adequate for the purpose of diagnostics (Franceschini et al., 2014).

respectively at (i) identifying inconsistent localizations and (ii) identifying and (temporarily) excluding purportedly faulty sensors.

2.2 Mathematical model for target localization

This section briefly recalls a recent mathematical model for target localization, when using combinations of LVM systems equipped with sensors of different nature. In general, each i-th LVM system (S_i) includes a number of sensors; we conventionally indicate the generic j-th sensor of S_i as s_{ij} (e.g., s_{i1}, s_{i2}, …, s_{ij}, …). Sensors can be classified in two typologies:

- *distance* sensors, able to measure their distance (d_{ij}) from the target (see Figure A.2, in the appendix);
- *angular* sensors, able to measure the azimuth (θ_{ij}) and elevation (φ_{ij}) angle subtended by the target (see Figure A.2, in the appendix).

Assuming that P is the point to be localized in the 3D space (e.g., the centre of a spherical target), the localization problem may be formulated through the following linear (or linearized) model (Galetto et al., 2015; Franceschini et al., 2016):

$$\boldsymbol{A}\cdot\boldsymbol{X}-\boldsymbol{B}\equiv\begin{bmatrix}\boldsymbol{A}^{dist}\\ \boldsymbol{A}^{ang}\end{bmatrix}\cdot\boldsymbol{X}-\begin{bmatrix}\boldsymbol{B}^{dist}\\ \boldsymbol{B}^{ang}\end{bmatrix}=0\,, \tag{2}$$

where $\boldsymbol{X}=[X, Y, Z]^T$ is the position vector of P in a global Cartesian coordinate system $OXYZ$; $\boldsymbol{A}^{dist}$, $\boldsymbol{A}^{ang}$ and $\boldsymbol{B}^{dist}$, $\boldsymbol{B}^{ang}$ are respectively the so-called *design* and *reduced measured observation* matrices, both referred to $OXYZ$ (Wolberg, 2005). The matrices related to distance sensors are labelled with superscript "*dist*", while those related to angular sensors with superscript "*ang*". $\boldsymbol{A}$ and $\boldsymbol{B}$ contain several parameters related to each generic (ij)-th sensor: the position/orientation parameters ($X_{0_{ij}}, Y_{0_{ij}}, Z_{0_{ij}}$ and ω_{ij}, ϕ_{ij}, κ_{ij}) and the distance (d_{ij}) and/or angles (θ_{ij}, φ_{ij}) subtended by the target, with respect to a local Cartesian coordinate system $o_{ij}x_{ij}y_{ij}z_{ij}$. Since the "true" values of the above parameters are never known exactly, they can be replaced with appropriate estimates: $\hat{X}_{0_{ij}}, \hat{Y}_{0_{ij}}, \hat{Z}_{0_{ij}}$, $\hat{\omega}_{ij}$, $\hat{\phi}_{ij}$ and $\hat{\kappa}_{ij}$ resulting from initial calibration process(es),

$\hat{d}_{ij}$ resulting from distance measurements, and $\hat{\theta}_{ij}$ and $\hat{\varphi}_{ij}$ resulting from angular measurements. For details on the construction of $\boldsymbol{A}$ and $\boldsymbol{B}$, see Sect. A1 (in the appendix).

The unknown coordinates of *P* are determined solving the system in Eq. 2, which is generally *overdefined*, i.e. there are more equations than unknown parameters: one for each distance sensor and two for each angular sensor.

The equations of the system may differently contribute to the uncertainty in the localization of *P*. Three important factors affecting this uncertainty are:

1. *Uncertainty in the local measurements* ($\hat{d}_{ij}$, $\hat{\theta}_{ij}$ and $\hat{\varphi}_{ij}$) by sensors, which generally depends on their metrological characteristics;
2. *Relative position* between *P* and each sensor; e.g., for angular sensors, the uncertainty in the localization of *P* increases proportionally to the distance between *P* and the sensors (Maisano and Mastrogiacomo, 2016);
3. *Uncertainty in the position/orientation of sensors*, resulting from initial calibration process(es).

For simplicity, the proposed mathematical model considers only the first two factors, neglecting the third one (Maisano and Mastrogiacomo, 2016).

Having said that, it would be appropriate to solve the system in Eq. 2 giving greater weight to the contributions from the sensors producing less uncertainty and *vice versa*. To this purpose, a practical method is that of *Generalized Least Squares* (GLS) (Franceschini et al., 2011; Kariya and Kurata, 2004), in which a weight matrix ($\boldsymbol{W}$), which takes into account the uncertainty produced by the equations, is defined as:

$$\boldsymbol{W} = \left[\boldsymbol{J} \cdot \left(\boldsymbol{cov}(\xi)\right) \cdot \boldsymbol{J}^T\right]^{-1}, \tag{3}$$

where $\boldsymbol{J}$ is the Jacobian matrix containing the partial derivatives of the elements in the first member of Eq. 2 (i.e., $\boldsymbol{A}\cdot\boldsymbol{X} - \boldsymbol{B}$) with respect to the sensors' local measurements (contained in the vector $\boldsymbol{\xi}$), and $\boldsymbol{cov}(\boldsymbol{\xi})$ is the relevant covariance matrix. For details, see Sect. A1 in the appendix.

Assuming that sensors work independently from each other and there is no correlation between the local measurements related to different sensors, $\boldsymbol{cov(\xi)}$ is a diagonal matrix containing the variances related to these measurements. Variances can be determined in several ways: (i) from manuals or technical documents relating to the sensors in use, (ii) estimated through *ad hoc* experimental tests, or (iii) estimated using data from previous calibration processes. We remark that these values should reflect the sensors' uncertainty in realistic working conditions, e.g., in the presence of vibrations, light/temperature variations and other typical disturbance factors.

By applying the GLS method to the system in Eq. 3, we obtain the final estimate of $\boldsymbol{X}$ as:

$$\hat{\boldsymbol{X}} = \left(\boldsymbol{A}^T \cdot \boldsymbol{W} \cdot \boldsymbol{A}\right)^{-1} \cdot \boldsymbol{A}^T \cdot \boldsymbol{W} \cdot \boldsymbol{B} \,. \tag{4}$$

For further details on the GLS method, see (Kariya and Kurata, 2004).

3. On-line diagnostic tests

This section is organized into two subsections: Sect. 3.1 describes a *global* test to evaluate the consistency of a target localization, while Sect. 3.2 describes a *local* test that – when a target localization is not considered consistent by the global test – identifies the potentially faulty sensor(s) and (temporarily) excludes them from the localization process, without interrupting it.

Before going into the discussion of the tests, we define the *residuals* of the sensor local measurements as the difference between the measured quantities (labelled with the symbol "^") and those calculated using the coordinates of *P*, resulting from the localization process (see Eqs. A3 and A7, in the appendix):

$$\left.\begin{aligned} \varepsilon_{d_{ij}} &= \hat{d}_{ij} - d_{ij} \\ \varepsilon_{\theta_{ij}} &= \hat{\theta}_{ij} - \theta_{ij} \\ \varepsilon_{\varphi_{ij}} &= \hat{\varphi}_{ij} - \varphi_{ij} \end{aligned}\right\} \begin{array}{l} \text{for distance sensors} \\ \text{for angular sensors} \end{array} . \tag{5}$$

In the absence of systematic error causes, it is reasonable to hypothesize that these residuals follow zero-mean normal distributions: $\varepsilon_{d_{ij}} \sim N\left(\mu_{d_{ij}} \approx 0, \sigma^2_{d_{ij}}\right)$, $\varepsilon_{\theta_{ij}} \sim N\left(\mu_{\theta_{ij}} \approx 0, \sigma^2_{\theta_{ij}}\right)$ and $\varepsilon_{\varphi_{ij}} \sim N\left(\mu_{\varphi_{ij}} \approx 0, \sigma^2_{\varphi_{ij}}\right)$; these hypotheses will be tested experimentally. The dispersion of residuals (depicted by the relevant variances $\sigma^2_{d_{ij}}, \sigma^2_{\theta_{ij}}$ and $\sigma^2_{\varphi_{ij}}$) depends on the technical/metrological characteristics of sensors; e.g., measurements performed using technologically advanced sensors, such as the interferometer or Absolute Distance Meter (ADM) of a laser tracker, are likely to be less dispersed than those performed using relatively coarse sensors, such as ultrasonic distance sensors or low-end photogrammetric cameras.

Assuming that $\sigma^2_{d_{ij}}, \sigma^2_{\theta_{ij}}$ and $\sigma^2_{\varphi_{ij}}$ are known, residuals can be standardized as follows:

$$\left.\begin{aligned} z_{d_{ij}} &= \frac{\varepsilon_{d_{ij}} - \mu_{d_{ij}}}{\sigma_{d_{ij}}} \approx \frac{\varepsilon_{d_{ij}}}{\sigma_{d_{ij}}} \\ z_{\theta_{ij}} &= \frac{\varepsilon_{\theta_{ij}} - \mu_{\theta_{ij}}}{\sigma_{\theta_{ij}}} \approx \frac{\varepsilon_{\theta_{ij}}}{\sigma_{\theta_{ij}}} \\ z_{\varphi_{ij}} &= \frac{\varepsilon_{\varphi_{ij}} - \mu_{\varphi_{ij}}}{\sigma_{\varphi_{ij}}} \approx \frac{\varepsilon_{\varphi_{ij}}}{\sigma_{\varphi_{ij}}} \end{aligned}\right\} \begin{array}{l} \text{for distance sensors} \\ \\ \text{for angular sensors} \end{array} . \quad (6)$$

The resulting standardized residuals are, by definition, normally distributed random variables with zero mean and unit variance: $z_{d_{ij}}, z_{\theta_{ij}}, z_{\varphi_{ij}} \sim N(0, 1)$.

3.1 Global test

The first diagnostic criterion is aimed at identifying the non-plausible localizations of *P*. The standardized residuals related to the sensors involved in the target localization (see Eq. 6) are aggregated into the *standardized residual sum of squares* (*SRSS*) indicator:

$$SRSS(P) = \sum_{ij \in I^{dist}} z^2_{d_{ij}} + \sum_{ij \in I^{ang}} \left(z^2_{\theta_{ij}} + z^2_{\varphi_{ij}}\right) = \sum_{ij \in I^{dist}} z^2_{d_{ij}} + \sum_{ij \in I^{ang}} z^2_{\theta_{ij}} + \sum_{ij \in I^{ang}} z^2_{\varphi_{ij}} , \quad (7)$$

where I^{dist} and I^{ang} are the sets of index-pair values (ij), relating to the sensors able to perform distance and angular measurements respectively. In general, these types of local measurements are mutually exclusive, since sensors able to measure distances are not able to measure angles and *vice versa*.

By definition, $SRSS(P) \geq 0$ for all the points (P) in the measurement volume. Since the localization problem is overdetermined and sensor measurements are naturally dispersed, a solution that exactly satisfies all distance and angular constrains (i.e., $SRSS(P) = 0$) is not realistically possible.

In a broader perspective, $SRSS(P)$ is the sum of $|I^{dist}|$, $|I^{ang}|$ and $|I^{ang}|$ squared realizations (the symbol "| |" denotes the cardinality of a set) of the zero-mean and unit-variance normally distributed random variables $z_{d_{ij}}, z_{\theta_{ij}}, z_{\varphi_{ij}}$. $SRSS(P)$ can therefore assume the following form:

$$SRSS(P) = \chi^2_{d_{ij}} + \chi^2_{\theta_{ij}} + \chi^2_{\varphi_{ij}}, \tag{8}$$

where:

$\chi^2_{d_{ij}}$, $\chi^2_{\theta_{ij}}$ and $\chi^2_{\varphi_{ij}}$ are three chi-square distributed random variables, with respectively $|I^{dist}|$, $|I^{ang}|$ and $|I^{ang}|$ degrees of freedom (DoF), since they are obtained by summing independent terms;

$SRSS(P)$ is a new chi-square distributed random variable with $|I^{dist}| + |I^{ang}| + |I^{ang}| = |I^{dist}| + 2\cdot|I^{ang}|$ DoF, since it is obtained by adding the three above chi-square distributed variables (Ross, 2009).

Every time the localization of a target is performed, diagnostics calculates the quantity $SRSS(P)$. Assuming a risk α as a type-I error, a one-sided confidence interval for $SRSS(P)$ can be calculated in order to test the consistency of the localization; $\chi^2_{\nu,1-\alpha}$ is the upper limit of this interval, considering a chi-square distribution with $\nu = |I^{dist}| + 2\cdot|I^{ang}|$ DoF and a $(1-\alpha)$ confidence level.

The test drives to the following two alternative conclusions:

$SRSS(P) \leq \chi^2_{\nu,1-\alpha}$ → localization is considered consistent;

$SRSS(P) > \chi^2_{\nu,1-\alpha}$ → localization is considered inconsistent, hence it is rejected.

3.1.1 Set up of test parameters

The risk level α is established by the user. A high α prevents from dubious localizations, although it might drive to reject good ones. On the other hand, a low α speeds up the localization process, although it might drive to collect wrong data due to the consequent increase of the type-II error (β).

The variances of residuals – which are essential for calculating the standardized residuals – can be determined empirically, localizing a sample of *M* points randomly distributed in the measurement volume, in the absence of systematic error sources. For each *k*-th point, the three types of residuals defined in Eq. 5 can be calculated: $\varepsilon_{d_{ij}}$, $\varepsilon_{\theta_{ij}}$ and $\varepsilon_{\varphi_{ij}}$. The number of residuals of each type may change depending on the number of sensors involved in each *k*-th localization, which is in turn influenced by their communication range and relative position with respect to *P* (Maisano and Mastrogiacomo, 2016).

In the absence of systematic error causes and time or spatial/directional effects, it is reasonable to assume that homologous residuals – i.e., residuals concerning the same type of measured quantity ($\hat{d}_{ij}$, $\hat{\theta}_{ij}$ and $\hat{\varphi}_{ij}$), from sensors of the same (*i*-th) LVM system – are zero-mean normally distributed random variables with the same dispersion. This is justified by the fact that the local-measurement dispersion of sensors is closely related to their technical and metrological characteristics.

Therefore, the mean values and variances of the residuals of the problem are reduced to:

$$\begin{aligned} &\mu_{d_{i\bullet}}, \sigma^2_{d_{i\bullet}} \text{ for the } \varepsilon_{d_{ij}} \text{ residuals} \\ &\mu_{\theta_{i\bullet}}, \sigma^2_{\theta_{i\bullet}} \text{ for the } \varepsilon_{\theta_{ij}} \text{ residuals} \\ &\mu_{\varphi_{i\bullet}}, \sigma^2_{\varphi_{i\bullet}} \text{ for the } \varepsilon_{\varphi_{ij}} \text{ residuals} \end{aligned} \quad (9)$$

where the subscript "i•" indicates that these parameters are calculated aggregating the residuals related to sensors from the i-th LVM system (S_i), considering the totality of the localizations of the M points available. The resulting mean values can be used to test the hypothesis of zero-mean distributions, while the variances can be used to determine the standardized residuals for the test (see Eq. 6).

3.1.2 First experimental example

In a first example, let us consider a specific combination of two LVM prototype systems:

(S_1) MScMS-I, i.e., a system consisting of multiple ultrasonic sensors – denominated Crickets (Franceschini et al., 2010) – which are able to measure their distance from the target;

(S_2) MScMS-II, i.e., a system consisting of different toy cameras – PixArt/WiiMote infrared cameras, with 126·96 pixels resolution and 100 fps – which are able to measure the angles subtended by the target (Franceschini et al., 2011).

Both systems have been designed and developed at Politecnico di Torino - DIGEP and include inexpensive but not very accurate sensors, e.g., the typical distance-measurement uncertainty of Crickets is of the order of a few millimetres (Franceschini et al ., 2010), while the angular-measurement uncertainty of the toy cameras is of the order of some tenths of a degree (Maisano and Mastrogiacomo, 2016).

We set up a distributed LVM "macro-system" consisting of 5 Crickets (i.e., s_{11}, s_{12}, s_{13}, s_{14} and s_{15}) and 3 toy cameras (i.e., s_{21}, s_{22} and s_{23}) with known positions and orientations, which are distributed around the measurement volume, as schematized in Figure 1.

The variances of the residuals were estimated empirically, considering a sample of about $M = 50$ points, which are randomly distributed in the measurement volume. The localization of these points was performed in a controlled environment (e.g., temperature, light and vibrations were kept under control) and the distributions of residuals were thoroughly analyzed, in order to exclude measurement accidents, e.g., time or spatial/directional effects, or non-random causes of variation in general.

Since all the MScMS-I distance sensors as well as the MScMS-II angular sensors are nominally identical, residuals can be grouped into 3 sets: one (including the $\varepsilon_{d_{1j}}$ residuals) for the distance sensors from S_1, and two (including the $\varepsilon_{\theta_{2j}}$ and $\varepsilon_{\varphi_{2j}}$ residuals) for the angular sensors from S_2. The zero-mean normal distribution of these sets of residuals was verified by the Anderson-Darling normality test at $p < 0.05$ (Ross, 2009).

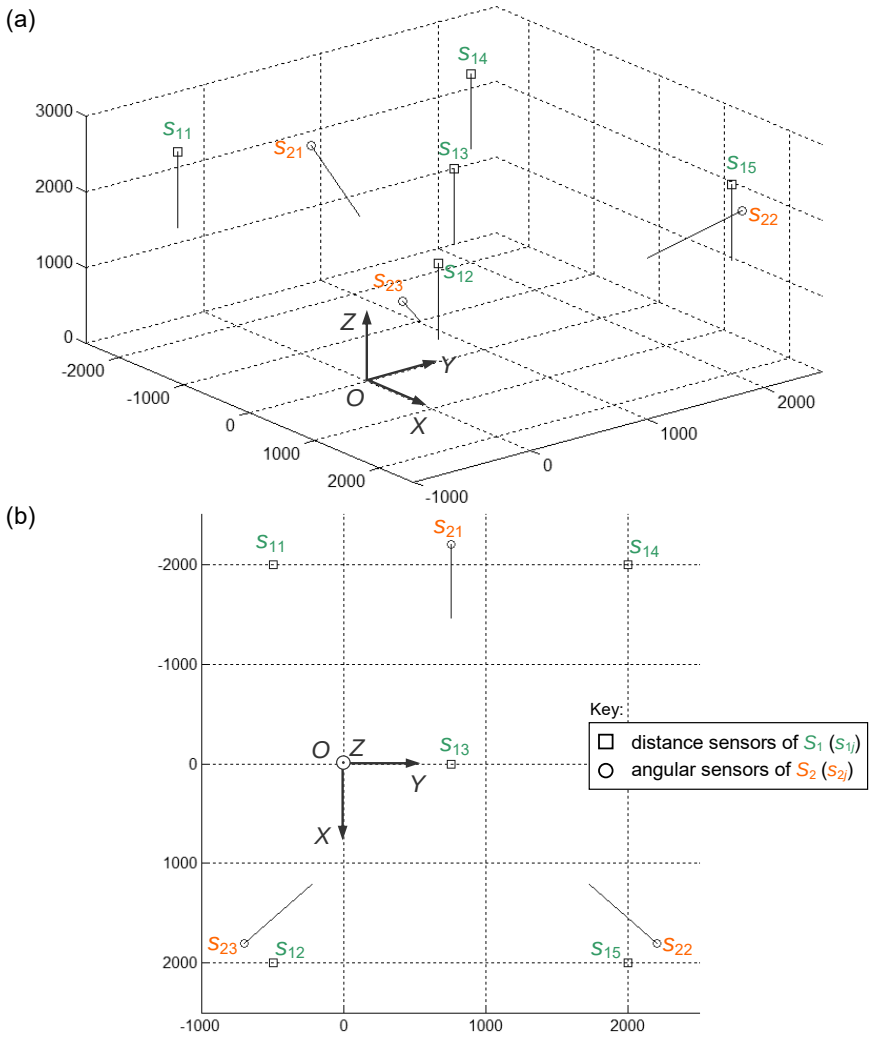

Figure 1. Representation of the position and orientation of the distance (s_{1j}) and angular (s_{2j}) sensors in use in the first experimental example: (a) 3D view and (b) *XY* plane view. *OXYZ* is the global coordinate system (coordinates in millimetres). The outgoing vectors (in blue) represent the sensor orientations.

Table 1 reports the mean and standard-deviation values estimated for these sets of residuals.

Residuals	Sensors	Number	Mean value	Variance
$\varepsilon_{d_{1j}}$	s_{11}, s_{12}, s_{13}, s_{14} and s_{15}	5·50 = 250	$\hat{\mu}_{d_{1\bullet}}$ = -0.05 mm	$\hat{\sigma}^2_{d_{1\bullet}}$ = 3.38 mm^2
$\varepsilon_{\theta_{2j}}$	s_{21}, s_{21} and s_{23}	3·50 = 150	$\hat{\mu}_{\theta_{2\bullet}}$ = 0.02 deg	$\hat{\sigma}^2_{\theta_{2\bullet}}$ = 0.083 deg^2
$\varepsilon_{\varphi_{2j}}$	*idem*	*idem*	$\hat{\mu}_{\varphi_{2\bullet}}$ = -0.038 deg	$\hat{\sigma}^2_{\varphi_{2\bullet}}$ = 0.090 deg^2

Table 1. Estimated mean value and variance related to the local-measurement residuals, in the first experimental example.

In conditions of maximum visibility – i.e., all the 5 distance sensors and 3 angular sensors are able to see the target P – the confidence-interval limit for *SRSS*, assuming a type-I risk level $\alpha = 0.05$ and $\nu = |I^{dist}| + 2\cdot|I^{ang}| = 5 + 2\cdot 3 = 11$ DoF, becomes:

$$SRSS(P) \le \chi^2_{\nu=11,1-\alpha=0.95} \Rightarrow SRSS(P) \le 19.7\,. \tag{10}$$

Let us now consider a possible accident that can occur using ultrasonic sensors. Referring to the representation in Figure 2, suppose that an obstacle, for example an operator who performs the measurement, is interposed between P and two of the distance sensors (i.e., s_{12} and s_{13}), blocking them. At the same time, the ultrasonic signal reflection on the floor/ceiling of the workshop produces two wrong measurements. Consequently, the distance measurements by s_{12} and s_{13} are significantly overestimated. Also, it is assumed that the remaining sensors are able to perform their local measurements correctly; see the example in Table 2(a).

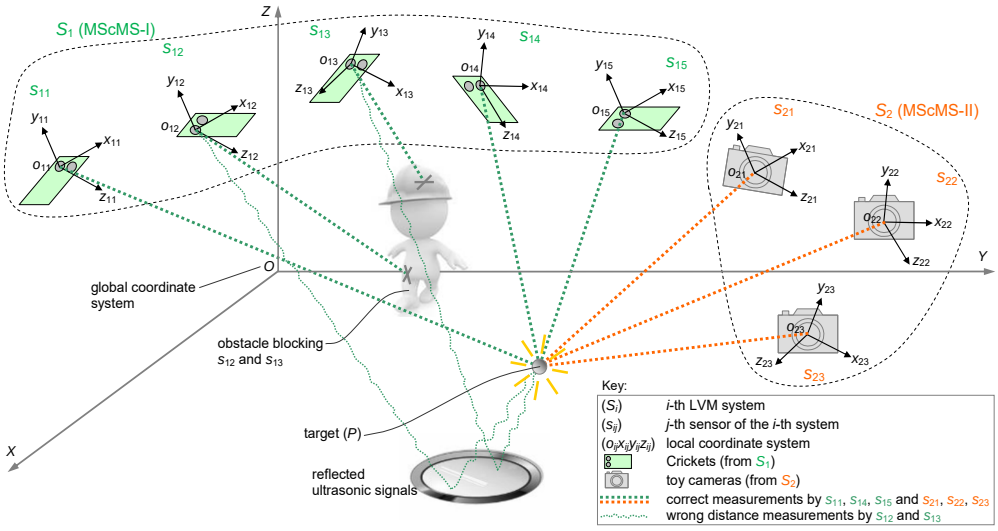

Figure 2. Scheme of the set-up in the first experimental example. A measurement accident in two (ultrasonic) sensors (i.e., s_{12} and s_{13}) of S_1 causes wrong distance measurements (d_{12} and d_{13}).

In this case, the mathematical model will produce the following (distorted) localization solution: $P \equiv (-99.9, 1449.7, 21.2)$ [mm], which is characterized by a high error: $SRSS(P) \approx 1.2 \cdot 10^5 > 19.7$. Owing to this result, the global test suggests that this localization is inconsistent.

Sensor	(a) Accident present			(b) Accident removed		
	d_{ij} [mm]	θ_{ij} [deg]	φ_{ij} [deg]	d_{ij} [mm]	θ_{ij} [deg]	φ_{ij} [deg]
s_{11}	3272.6	N/A	N/A	3274.6	N/A	N/A
s_{12}	(wrong) 4236.5	N/A	N/A	(correct) 2814.9	N/A	N/A
s_{13}	(wrong) 3196.3	N/A	N/A	(correct) 1970.4	N/A	N/A
s_{14}	3314.0	N/A	N/A	3318.1	N/A	N/A
s_{15}	2857.1	N/A	N/A	2856.8	N/A	N/A
s_{21}	N/A	13.37	-29.36	N/A	13.42	-29.36
s_{22}	N/A	-10.33	-34.35	N/A	-10.23	-34.46
s_{23}	N/A	122.80	-35.86	N/A	122.91	-35.83

Table 2. Example of local measurements by the sensors of a combination of two LVM systems (S_1 and S_2) in the first experimental example: (a) in the presence of an accident causing wrong distance measurements by s_{12} and s_{13} and (b) after removing the cause of the accident.

After removing the obstacle, the new distances related to s_{12} and s_{13} are respectively $d_{12} = 4236.5$ mm and $d_{13} = 3196.3$ mm, while the local measurements relating to the remaining sensors are almost identical to the previous ones (see Table 2(b)). The new localization is: $P \equiv (352.7, 698.6, 560.6)$ [mm]. The corresponding *SRSS* value is $SRSS(P) \approx 4.44 \leq 19.7$. Hence, the new localization can be considered consistent.

3.1.3 Second experimental example

Let us consider a second example in which two LVM systems include sensors with relatively high metrological characteristics. Precisely, these two systems are:

(S_1) a distributed photogrammetric system consisting of three Hitachi Gigabit Ethernet photogrammetric infrared cameras (s_{11}, s_{12} and s_{13}) – pixel resolution: 1360x1024, frame rate: 30 fps (Hitachi Kokusai Electric Inc., 2016) – using a 38.1 mm reflective spherical target. Each camera is able to provide the azimuth (θ_{11}, θ_{12}, and θ_{13}) and elevation (φ_{11}, φ_{12}, and φ_{13}) angular measurements with respect to the target P;

(S_2) a laser tracker API Radian™ (API, 2016) with a Spherically Mounted Retroreflector (SMR) of the same diameter of the target of S_1. S_2 is equipped with an ADM (s_{21}), providing distance measurements (d_{21}) and an angular sensor (s_{22}), providing two angular measurements – i.e., azimuth (θ_{22}) and elevation (φ_{22}) – of P. The local Cartesian coordinate systems of the two sensors are coincident.

We set up a distributed LVM "macro-system" consisting of total 5 sensors (i.e., s_{11}, s_{12}, s_{13}, s_{21} and s_{22}) with known positions and orientations, which are distributed around the measurement volume, as schematized in Figure 3.

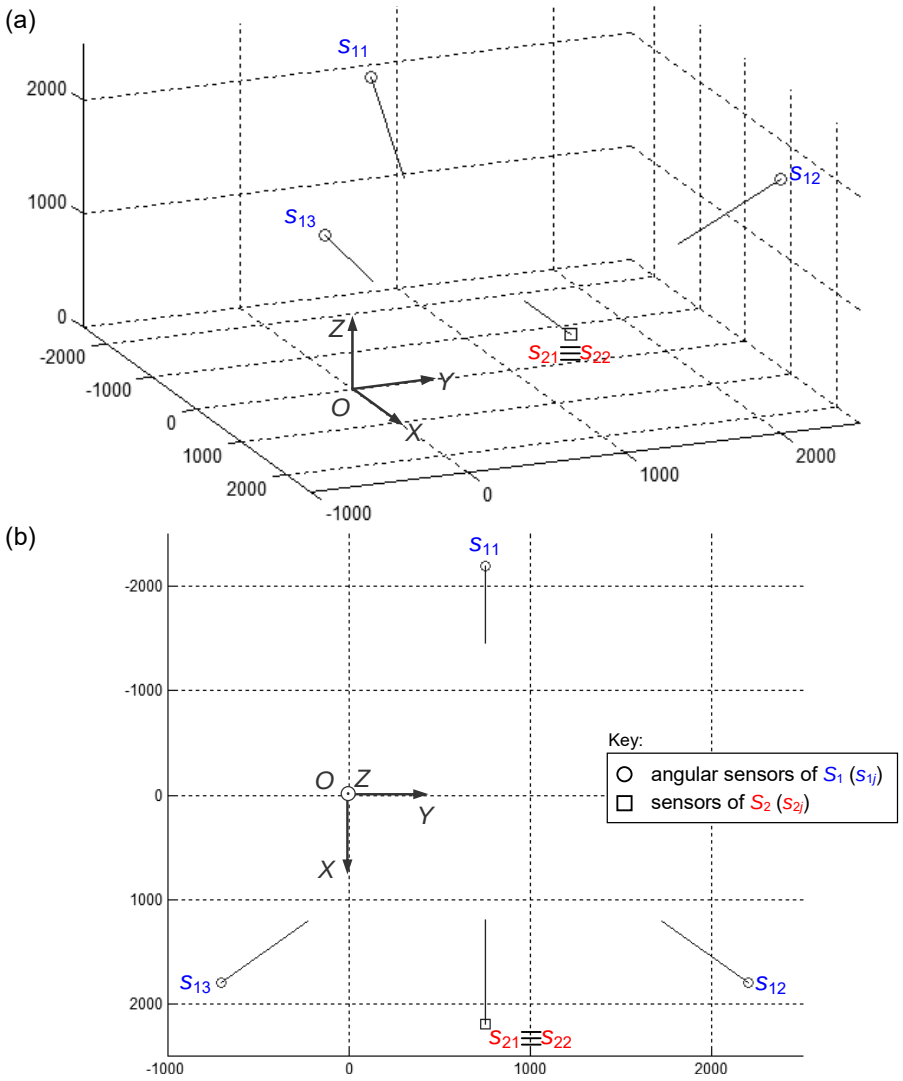

Figure 3. Representation of the position and orientation of the photogrammetric cameras (s_{1j}) and the laser-tracker distance (s_{21}) and angular (s_{22}) sensors in use in the second experimental example: (a) 3D view and (b) *XY* plane view. *OXYZ* is the global coordinate system (coordinates in millimetres). The outgoing vectors (in blue) represent the sensor orientations.

The proposed localization model is able to estimate the 3D position of each measured point, based on the 9 local measurements available (i.e., two angular measurements for each of the three photogrammetric cameras; two angular measurements and one distance measurement for the laser tracker).

The mean values and variances related to the local-measurement residuals were estimated on the basis of the localization of $M = 50$ points, which are randomly distributed in the measurement volume. The resulting values are reported in Table 3.

Residuals	Sensors	Number	Mean value	Variance
$\varepsilon_{\theta_{1j}}$	s_{11}, s_{12} and s_{13}	3·50 = 150	$\hat{\mu}_{\theta_{1\bullet}} = 1.9\cdot10^{-4}$ deg	$\hat{\sigma}^2_{\theta_{1\bullet}} = 2.5\cdot10^{-4}$ deg^2
$\varepsilon_{\varphi_{1j}}$	*idem*	3·50 = 150	$\hat{\mu}_{\varphi_{1\bullet}} = 2.0\cdot10^{-4}$ deg	$\hat{\sigma}^2_{\varphi_{1\bullet}} = 2.6\cdot10^{-4}$ deg^2
$\varepsilon_{d_{2j}}$	s_{21}	50	$\hat{\mu}_{d_{1\bullet}} = -4.5\cdot10^{-7}$ mm	$\hat{\sigma}^2_{d_{1\bullet}} = 9.1\cdot10^{-11}$ mm^2
$\varepsilon_{\theta_{2j}}$	s_{22}	50	$\hat{\mu}_{\theta_{2\bullet}} = 1.1\cdot10^{-3}$ deg	$\hat{\sigma}^2_{\theta_{2\bullet}} = 3.7\cdot10^{-3}$ deg^2
$\varepsilon_{\varphi_{2j}}$	*idem*	50	$\hat{\mu}_{\varphi_{2\bullet}} = 8.7\cdot10^{-3}$ deg	$\hat{\sigma}^2_{\varphi_{1\bullet}} = 1.7\cdot10^{-3}$ deg^2

Table 3. Estimated mean value and variance related to the local-measurement residuals, in the second experimental example.

In conditions of maximum visibility (i.e., when the totality of the sensors can see the target) and assuming a type-I risk level $\alpha = 0.05$ and $\nu = 2\cdot3 + 1 + 1\cdot2 = 9$ DoF, the confidence-interval limit for *SRSS* becomes:

$$SRSS(P) \leq \chi^2_{\nu=9,1-\alpha=0.95} \Rightarrow SRSS(P) \leq 16.9 . \quad (11)$$

Suppose that a possible accident produces a distortion in the angles measured by the angular encoder of the laser tracker (s_{22}), while the distance sensor (s_{21}) performs the measurement correctly (see the representation in Figure 4). Moreover, suppose that the three photogrammetric cameras (s_{11}, s_{12} and s_{13}) are able to measure the angles subtended by P correctly (see Table 4).

In this case, the localization algorithm will produce the following (distorted) localization solution: $P \equiv (1964.9, 1254.5, 946.5)$ [mm], characterized by a high error, i.e., $SRSS(P) \approx 3.6\cdot10^3 > 16.9$. This diagnostic test therefore suggests to reject the localization result.

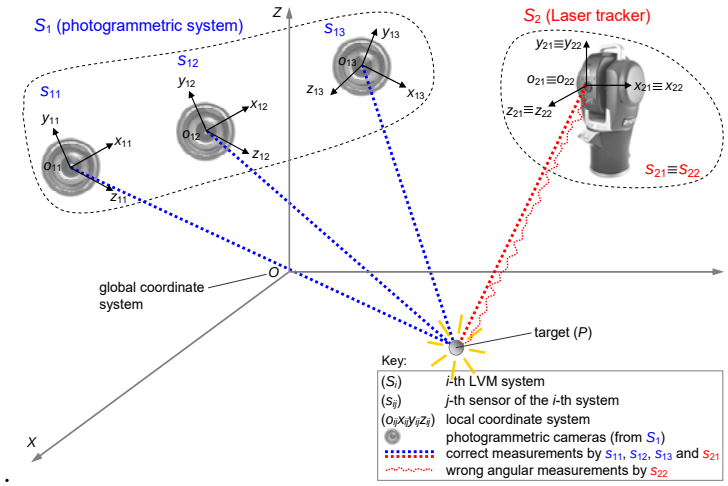

Figure 4. Scheme of the set-up in the second experimental example. A measurement accident in the laser-tracker angular sensor (s_{22}) causes the wrong measurement of the azimuth (θ_{22}) and elevation (φ_{23}) angles.

Sensor	(a) Accident present			(b) No accident		
	d_{ij} [mm]	θ_{ij} [deg]	φ_{ij} [deg]	d_{ij} [mm]	θ_{ij} [deg]	φ_{ij} [deg]
s_{11}	N/A	62.16	-13.91	N/A	62.17	-13.79
s_{12}	N/A	96.95	-47.04	N/A	96.91	-47.07
s_{13}	N/A	-14.82	-27.82	N/A	-14.79	-27.80
s_{21}	559.2	N/A	N/A	559.2	N/A	N/A
s_{22}	N/A	(wrong) 25.96	(wrong) -7.39	N/A	(correct) 30.96	(correct) -3.39

Table 4. Example of local measurements by the sensors of a combination of two LVM systems (S_1 and S_2) in the second experimental example: (a) before and (b) after removing the cause of the measurement accident.

Repeating the measurement after having eliminated the anomaly in s_{22}, the new angles measured by s_{22} are $\theta_{22} = 30.96$ degrees and $\varphi_{22} = -3.39$ degrees respectively, while those relating to the remaining sensors are almost identical to the previous ones (see Table 2(b)). The new localization is: $P \equiv (1952.3,\ 1250.3,\ 966.9)$ [mm]. The corresponding *SRSS* value is $SRSS(P) \approx 5.23 \leq 16.9$. Hence, the new localization can be considered consistent.

3.2 Local test

If the global test fails, a local test can be performed for failure isolation. The philosophy of this other test is to correct the results of a dubious localization, by

excluding the purportedly faulty sensor(s), without losing the observations from the remaining sensors. In this way, the target localization process is not interrupted, even in the presence of local anomalies.

Referring to the local measurements by each (*ij*)-th sensor, we now consider the three types of standardized residuals, which are defined in Eq. 6 ($z_{d_{ij}}$, $z_{\theta_{ij}}$, and $z_{\varphi_{ij}}$). These residuals can be used for outlier detection with uncorrelated and normally distributed observations: if the local measurement is not an outlier, then the corresponding standardized residual will be normally distributed $\sim N(0, 1)$. Each standardized residual is compared to a $\alpha/2$-quantile and a $(1 - \alpha/2)$-quantile of the standard normal distribution (i.e., $z_{\alpha/2}$ and $z_{1-\alpha/2}$), with the significance level α. The null-hypothesis, which denotes that the (*ij*)-th local measurement is not an outlier, is rejected if the standardized residual is not included in the $[z_{\alpha/2}, z_{1-\alpha/2}]$ symmetrical confidence interval. An outlier in one standardized residual generally causes ones other residuals to be increased in absolute values.

Local testing is easy under the assumption that there is only one purportedly faulty sensor (or outlier) in the current localization: the local measurement with the largest (absolute value of the) standardised residual, provided that it is beyond the confidence interval, is regarded as an outlier and the corresponding sensor (s_{ij}) is excluded from the localization problem.

The assumption that there is only one outlier is a severe restriction in the case measurements from more than one sensor are degraded. However, the procedure can be extended to multiple outliers iteratively: after the exclusion of a potentially faulty sensor, the statistical test and the rejection of one other sensor can be repeated until no more outliers are identified (Wieser et al., 2004).

3.2.1 Set up of test parameters

The standardized residuals that are used in this test are the same that are used in the global test; therefore they can be calculated according to the procedure described in Sect. 3.

3.2.2 First application example

Returning to the example presented in Sect. 3.1.2 – in which two distance sensors (s_{12} and s_{13}) perform distorted measurements – the relevant standardized residuals are reported in Table 5(a). These standardized residuals were determined using the residual variances estimated in Sect. 3.1.2.

Sensor	$z_{d_{ij}}$	$z_{\theta_{ij}}$	$z_{\varphi_{ij}}$
(a) Initial data			
s_{11}	136.49	N/A	N/A
s_{12}	(wrong) -149.21	N/A	N/A
s_{13}	(wrong) -206.22	N/A	N/A
s_{14}	-47.54	N/A	N/A
s_{15}	145.95	N/A	N/A
s_{21}	N/A	65.46	-41.44
s_{22}	N/A	-80.61	-32.47
s_{23}	N/A	-13.96	4.22
(b) s_{13} excluded			
s_{11}	48.04	N/A	N/A
s_{12}	(wrong) -241.97	N/A	N/A
s_{14}	-121.6	N/A	N/A
s_{15}	66.74	N/A	N/A
s_{21}	N/A	56.36	-24.54
s_{22}	N/A	-71.01	-13.74
s_{23}	N/A	-10.18	17.63
(c) s_{12} and s_{13} excluded			
s_{11}	0.76	N/A	N/A
s_{14}	0.79	N/A	N/A
s_{15}	0.25	N/A	N/A
s_{21}	N/A	-0.03	-0.05
s_{22}	N/A	1.33	-0.73
s_{23}	N/A	1.21	0.92

Table 5. Standardized residuals for the measurement exemplified in Sect. 3.1.2: (a) initial data, (b) data after the exclusion of sensor s_{12}, and (c) data after the exclusion of sensors s_{12} and s_{13}.

Assuming $\alpha = 5\%$, the confidence interval is $[z_{\alpha/2} = -1.96,\ z_{1-\alpha/2} = 1.96]$. All the residuals are outside this interval, but the "prime suspect" is s_{13}, being the sensor with the highest residual (absolute) value. s_{13} is then excluded and, repeating the localization, the new output is $P \equiv (-81.2,\ 1345.3,\ 358.2)$ [mm]. Despite this exclusion, all the residuals continue to be outside the confidence interval. In this other case the sensor with the highest residual (absolute) value is s_{12}, which is in turn excluded and the localization is repeated (see Table 5(b)). The new output is

$P \equiv (353.5,\ 694.9,\ 562.6)$ [mm] and all the standardized residuals are eventually contained within the confidence interval (see Table 5(c)).

Not surprisingly, the global test – which can be performed using the local measurements from the six remaining sensors only – is satisfied; precisely, $SRSS(P) = 5.9 \leq \chi^2_{\nu=9,1-\alpha=0.95} \cong 16.9$.

3.2.3 Second application example

Returning to the example presented in Sect. 3.1.3 – in which the two angles measured by the laser-tracker angular sensor (s_{22}) are distorted – the relevant standardized residuals are reported in Table 5(a). For this standardization, we used the residual variances ($\sigma^2_{d_1}$, $\sigma^2_{\theta_2}$ and $\sigma^2_{\varphi_2}$) that are reported in Sect. 3.1.3.

Sensor	$z_{d_{ij}}$	$z_{\theta_{ij}}$	$z_{\varphi_{ij}}$
(a) Initial data			
s_{11}	N/A	2.15	-9.67
s_{12}	N/A	39.15	-32.44
s_{13}	N/A	-19.87	-22.01
s_{21}	-0.01	N/A	N/A
s_{22}	N/A	(wrong) 74.64	(wrong) 36.11
(b) s_{22} excluded			
s_{11}	N/A	0.69	-1.23
s_{12}	N/A	-0.57	-0.11
s_{13}	N/A	-0.31	1.66
s_{21}	$-1.2*10^{-4}$	N/A	N/A

Table 6. Standardized residuals for the measurement exemplified in Sect. 3.2.2: (a) initial data and (b) data after the exclusion of sensor s_{22}.

Assuming $\alpha = 5\%$, the confidence interval is $[z_{\alpha/2} = -1.96,\ z_{1-\alpha/2} = 1.96]$. All the residuals are outside this interval, but the "prime suspect" is s_{22}, being the sensor with the highest residual (absolute) value. s_{22} is then excluded and, repeating the localization, the new output is $P \equiv (1952.3,\ 1250.3,\ 966.8)$ [mm] and all the standardized residuals are now contained within the confidence interval (see Table 5(b)).

Not surprisingly, the global test – which can be performed using the local measurements from the four remaining sensors – is also satisfied: $SRSS(P) = 4.91 \leq \chi^2_{\nu=7,1-\alpha=0.95} \cong 14.1$.

4. Conclusions

The on-line diagnostics presented in the paper makes it possible to monitor the target-localization consistency in real time, on the basis of some statistical tests. Tests are deliberately general and can be applied to any combination of LVM systems in which sensors (of different nature) perform distance and/or angular measurements. An important characteristic of these tests is their ability to selectively exclude faulty sensor(s), without interrupting the measurement process.

The proposed tests require the estimation of some parameters; primarily the variances related to the local-measurement residuals. These parameters can be evaluated empirically by performing some preliminary measurements under controlled conditions, according to the reasonable assumption of absence of time or spatial/directional effects. Data collected during the system set-up and calibration can be used for this purpose, with no additional effort (Bar-Shalom, et al., 2001).

Since the on-line implementation of these tests requires a certain computational capacity, it could slow down the target-localization process. However, this consequence is minimized due to (i) the high capacity of existing processors, (ii) the fact that the localization model in use is linearized, and (iii) test segmentation (i.e., the local test is performed only after the global test has detected the presence of potential anomalies). Some experimental tests showed that the response time required to implement these tests for individual measurements is in the order of magnitude of a few tenths of a second.

The proposed diagnostic tests can be applied in the localization of a unique target, which is seen by the sensors in use. In the absence of a *universal* target – i.e., a target able to be seen by sensors of different nature simultaneously (such as a laser tracker and a set of photogrammetric cameras) – it is possible to perform the localization

using different targets (such as a SMR for a laser tracker and a reflective spherical target for a set of photogrammetric cameras), repositioning them separately on the same support base. In this way, the local-measurement collection process is split into different phases, which involve sensors of different nature separately (e.g., the local measurements by photogrammetric cameras are collected in one phase, while those by laser tracker are collected in another one). This operation is not problematic for static measurements – in which the target(s) support base is fixed – but it is not feasible for dynamic measurements. Regarding the future, we plan to extend these tests and the proposed mathematical model for target-localization to the so-called 6-DOF probes equipped with multiple targets, which are visible from sensors of different nature (Maisano and Mastrogiacomo, 2018a; 2018b).

Acknowledgements

This research was supported by the project Co-LVM "Cooperative multi-sensor data fusion for enhancing Large-Volume Metrology applications", which is financed by Fondazione CRT, under the initiative "La Ricerca dei Talenti".

References

API (Automated Precision Inc.) (2016). RadianTM [accessed: 24-03-2016], http://www.apisensor.com.

Bai, O., Franceschini, F., Galetto, M., Mastrogiacomo, L., Maisano, D. (2014) A Comparison of Two Different Approaches to Camera Calibration in LSDM Photogrammetric Systems. In ASME (American Society of Mechanical Engineers) 2014 12th Biennial Conference on Engineering Systems Design and Analysis.

Bar-Shalom, Y., Li, X.R., Kirubarajan, T. (2001) Estimation with applications to tracking and navigation. Wiley, New York.

Chen, Z., et al. "A framework of measurement assisted assembly for wing-fuselage alignment based on key measurement characteristics." International Journal of Manufacturing Research 10.2 (2015): 107-128.

Estler, W.T., Edmundson, K.L., Peggs, G.N., Parker, D.H. (2002) Large-scale metrology—an update. CIRP Ann. Manuf. Technol., 51: 587-609.

Franceschini, F., Galetto, M., Maisano, D., Mastrogiacomo, L. (2009) On-line diagnostics in the Mobile Spatial coordinate Measuring System (MScMS). Precision Engineering, 33(4): 408-417.

Franceschini, F., Maisano, D., Mastrogiacomo, L., Pralio, B. (2010) Ultrasound transducers for large-scale metrology: a performance analysis for their use by the MScMS. Instrumentation and Measurement, IEEE Transactions on, 59(1): 110-121.

Franceschini, F., Galetto, M., Maisano, D., Mastrogiacomo, L., Pralio, B. (2011) Distributed Large-Scale Dimensional Metrology, Springer, London.

Franceschini, F., Maisano, D., Mastrogiacomo, L. (2014). Cooperative diagnostics for distributed large-scale dimensional metrology systems based on triangulation. Proceedings of the Institution of Mechanical Engineers, Part B: Journal of Engineering Manufacture, 228(4): 479-492.

Franceschini, F., Maisano, D. (2014). The evolution of large-scale dimensional metrology from the perspective of scientific articles and patents. The International Journal of Advanced Manufacturing Technology, 70(5-8), 887-909.

Franceschini, F., Galetto, M., Maisano, D., Mastrogiacomo, L. (2016). Combining multiple Large Volume Metrology systems: Competitive versus cooperative data fusion. Precision Engineering, 43: 514-524.

Galetto, M., Mastrogiacomo, L., Maisano, D., Franceschini, F. (2015). Cooperative fusion of distributed multi-sensor LVM (Large Volume Metrology) systems, CIRP Annals - Manufacturing Technology, 64(1): 483-486.

Gertler, J.J. (1998) Fault detection and diagnosis in engineering system. Marcel Dekker, NewYork.

Hall, B.D. (2004). On the propagation of uncertainty in complex-valued quantities. Metrologia, 41(3): 173.

Hartley, R., Zisserman, A. (2003) Multiple view geometry in computer vision. Cambridge University, 2nd edition, Cambridge (UK).

Hitachi Kokusai Electric Inc. (2016). GigE(Gigabit Ethernet) 3CCD Cameras [accessed: 24-03-2016], http://www.hitachi-kokusai.co.jp.

JCGM 200:2008 (2008) VIM—International vocabulary of metrology—basic and general concepts and associated terms (VIM). International Organization for Standardization, Geneva, Switzerland.

Kariya, T., Kurata, H. (2004) Generalized least squares, John Wiley & Sons, New York.

Maisano, D.A., Jamshidi, J., Franceschini, F., Maropoulos, P.G., Mastrogiacomo, L., Mileham, A., Owen, G. (2008). Indoor GPS: system functionality and initial performance evaluation. International Journal of Manufacturing Research, 3(3): 335-349.

Maisano, D., Mastrogiacomo, L. (2016). A new methodology to design multi-sensor networks for distributed large-volume metrology systems based on triangulation. Precision Engineering, 43, 105-118.

Maisano, D., Mastrogiacomo, L. (2018a). A novel multi-target modular probe for multiple Large-Volume Metrology systems. To appear on Precision Engineering, doi: 10.1016/j.precisioneng.2017.08.017.

Maisano, D., Mastrogiacomo, L. (2018b). Multi-Target Modular probe for Large-Volume Metrology. To appear on Recent Patents on Engineering, doi: 10.2174/1872121116661707261551l4.

Maropoulos, P.G., Muelaner, J.E., Summers, M.D., Martin, O.C. (2014) A new paradigm in large-scale assembly—research priorities in measurement assisted assembly. The International Journal of Advanced Manufacturing Technology, 70(1-4):621-633.

Peggs, G.N., Maropoulos, P.G., Hughes, E.B., Forbes, A.B., Robson, S., Ziebart, M., Muralikrishnan, B. (2009) Recent developments in large-scale dimensional metrology. Proceedings of the Institution of Mechanical Engineers, Part B: Journal of Engineering Manufacture, 223(6):571-595.

Ross, S.M. (2009). Introduction to probability and statistics for engineers and scientists. Academic Press.

Schmitt, R.H., Peterek, M., Morse, E., Knapp, W., Galetto, M., Härtig, F., ... & Estler, W.T. (2016). Advances in Large-Scale Metrology–Review and future trends. CIRP Annals-Manufacturing Technology, 65(2): 643-665.

Wieser, A., Petovello, M., Lachapelle, G. (2004) Failure Scenarios to be Considered with Kinematic High Precision Relative GNSS Positioning. Proc ION GNSS 2004, September 21-24. Long Beach, California, 1448-1459.

Wolberg, J. (2005) Data Analysis Using the Method of Least Squares: Extracting the Most Information from Experiments. Springer. ISBN 3-540-25674-1.

Appendix

A1. Details on the mathematical model for target localization

This section presents a detailed description of the mathematical model for target localization, when adopting combinations of LVM systems.

Let us consider a set of LVM systems (S_i, being $i = 1, 2, \ldots$), each of which is equipped with a number of sensors (s_{ij}, being $j = 1, 2, \ldots$) that are positioned around the object to be measured, with a local Cartesian coordinate system ($o_{ij}x_{ij}y_{ij}z_{ij}$), which is roto-translated with respect to a global Cartesian coordinate system *OXYZ* (see Figure A.1). The single LVM systems can be *centralized* or *distributed*; in the former case, sensors are rigidly connected to each other, while in the latter, they are not.

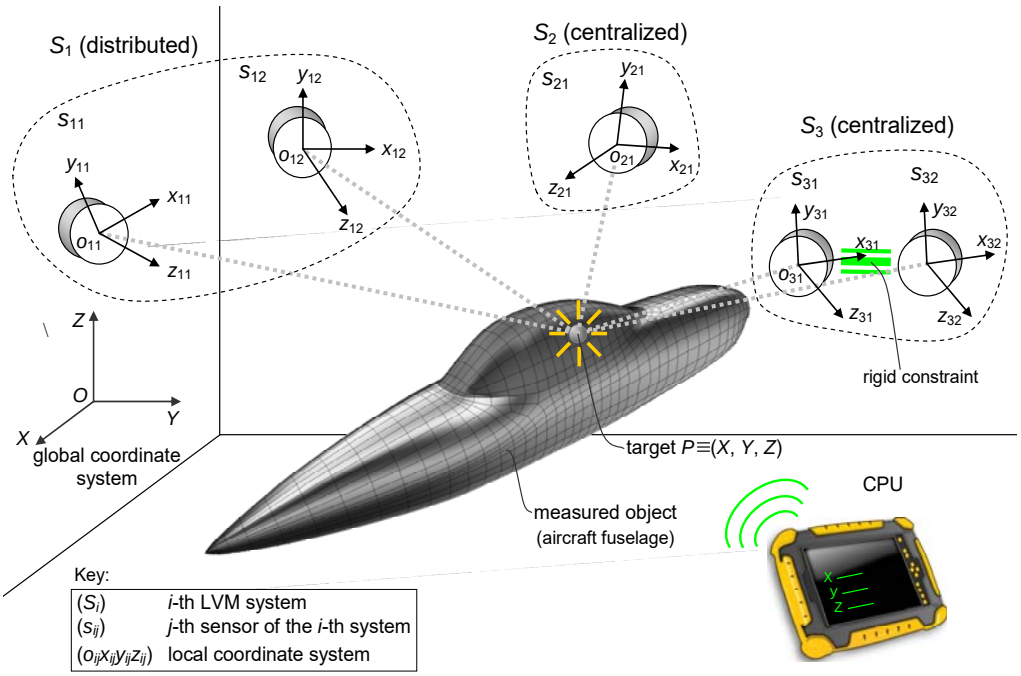

Figure A.1. Schematic representation of the combination of three LVM systems: S_1 is a distributed system with two sensors (s_{11} and s_{12}), while S_2 and S_3 are two centralized systems with one sensor (s_{21}) and two sensors (s_{31} and s_{32}) respectively.

A general transformation between a local and the global coordinate system is:

$$\boldsymbol{X} = \boldsymbol{R_{ij}}\boldsymbol{x_{ij}} + \boldsymbol{X_{0_{ij}}} \Rightarrow \begin{bmatrix} X \\ Y \\ Z \end{bmatrix} = \begin{bmatrix} r_{11_{ij}} & r_{12_{ij}} & r_{13_{ij}} \\ r_{21_{ij}} & r_{22_{ij}} & r_{23_{ij}} \\ r_{31_{ij}} & r_{32_{ij}} & r_{33_{ij}} \end{bmatrix} \begin{bmatrix} x_{ij} \\ y_{ij} \\ z_{ij} \end{bmatrix} + \begin{bmatrix} X_{0_{ij}} \\ Y_{0_{ij}} \\ Z_{0_{ij}} \end{bmatrix}. \quad \text{(A1)}$$

$\boldsymbol{R_{ij}}$ is a rotation matrix, which elements are functions of three rotation parameters:

$$\boldsymbol{R_{ij}} = \begin{bmatrix} \cos\phi_{ij}\cos\kappa_{ij} & -\cos\phi_{ij}\sin\kappa_{ij} & \sin\phi_{ij} \\ \cos\omega_{ij}\sin\kappa_{ij} + \sin\omega_{ij}\sin\phi_{ij}\cos\kappa_{ij} & \cos\omega_{ij}\cos\kappa_{ij} - \sin\omega_{ij}\sin\phi_{ij}\sin\kappa_{ij} & -\sin\omega_{ij}\cos\phi_{ij} \\ \sin\omega_{ij}\sin\kappa_{ij} - \cos\omega_{ij}\sin\phi_{ij}\cos\kappa_{ij} & \sin\omega_{ij}\cos\kappa_{ij} + \cos\omega_{ij}\sin\phi_{ij}\sin\kappa_{ij} & \cos\omega_{ij}\cos\phi_{ij} \end{bmatrix}, \quad \text{(A2)}$$

where ω_{ij} represents a counterclockwise rotation around the x_{ij} axis; ϕ_{ij} represents a counterclockwise rotation around the new y_{ij} axis, which was rotated by ω_{ij}; κ_{ij}

represents a counterclockwise rotation around the new z_{ij} axis, which was rotated by ω_{ij} and then ϕ_{ij}; for details, see (Franceschini et al., 2014).

$\boldsymbol{X}_{\boldsymbol{0}_{ij}} = \left[X_{0_{ij}}, Y_{0_{ij}}, Z_{0_{ij}}\right]^T$ are the coordinates of the origin of $o_{ij}x_{ij}y_{ij}z_{ij}$, in the global coordinate system *OXYZ*.

The (six) location/orientation parameters related to each (*ij*)-th sensor (i.e., $X_{0_{ij}}, Y_{0_{ij}}, Z_{0_{ij}}$, ω_{ij}, ϕ_{ij}, κ_{ij}) are treated as known parameters, since they are measured in an initial calibration process. This process, which may vary depending on the specific technology of the individual measuring systems, generally includes multiple measurements of calibrated artefacts, within the measurement volume (Bai et al, 2014).

The above considerations apply to both *distributed* and *centralized* LVM systems. In the latter case, sensors are rigidly connected (e.g., consider a photogrammetric tracking bar with three cameras), i.e., the position vectors of the individual sensors ($\boldsymbol{X}_{\boldsymbol{0}_{ij}}$) are linked to the respective $\boldsymbol{R}_{ij}$ matrices (rigid-body constraint).

The problem of localizing the point $P = [X, Y, Z]^T$ can be decomposed by considering distance and angular sensors separately, as discussed in Sects. A1.1 and A1.2 respectively.

A1.1 Distance sensors

From the local perspective of a generic (*ij*)-th distance sensor, the distance between $P = [X, Y, Z]^T$ and a local observation point – which is assumed to be coincident with the origin $o_{ij} = [\, X_{0_{ij}}, \; Y_{0_{ij}}, \; Z_{0_{ij}} \,]^T$ of the local coordinate system $o_{ij}x_{ij}y_{ij}z_{ij}$ – can be calculated as (see Figure A.2):

$$d_{ij} = \left\| \boldsymbol{X} - \boldsymbol{X}_{0_{ij}} \right\| = \sqrt{\left(X - X_{0_{ij}}\right)^2 + \left(Y - Y_{0_{ij}}\right)^2 + \left(Z - Z_{0_{ij}}\right)^2} \,. \tag{A3}$$

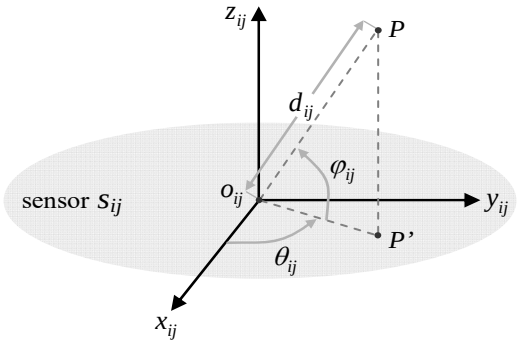

Figure A.2. For a generic sensor (s_{ij}), a distance (d_{ij}) and two angles – i.e., θ_{ij} (azimuth) and φ_{ij} (elevation) – are subtended by a line joining the point *P* (to be localized) and the origin o_{ij} of the local coordinate system $o_{ij}x_{ij}y_{ij}z_{ij}$.

Squaring both terms, we obtain

$$\left(X - X_{0_{ij}}\right)^2 + \left(Y - Y_{0_{ij}}\right)^2 + \left(Z - Z_{0_{ij}}\right)^2 - d_{ij}^2 = 0\,. \tag{A4}$$

Considering a point $\hat{\hat{\boldsymbol{X}}} = \left[\hat{\hat{X}}, \hat{\hat{Y}}, \hat{\hat{Z}}\right]^T$ that is reasonably close to $\boldsymbol{X}$, Eq. A4 can be linearized by a first order Taylor expansion[2]:

$$2 \cdot \begin{bmatrix} \hat{\hat{X}} - X_{O_{ij}} \\ \hat{\hat{Y}} - Y_{O_{ij}} \\ \hat{\hat{Z}} - Z_{O_{ij}} \end{bmatrix}^T \cdot \begin{bmatrix} X - \hat{\hat{X}} \\ Y - \hat{\hat{Y}} \\ Z - \hat{\hat{Z}} \end{bmatrix} = d_{ij}^2 - \left\{ \left(\hat{\hat{X}} - X_{0_{ij}}\right)^2 + \left(\hat{\hat{Y}} - Y_{0_{ij}}\right)^2 + \left(\hat{\hat{Z}} - Z_{0_{ij}}\right)^2 \right\} = 0\,. \tag{A5}$$

The above equation can be expressed in matrix form as:

$$\boldsymbol{A}_{\boldsymbol{ij}}^{\boldsymbol{dist}} \cdot \boldsymbol{X} - \boldsymbol{B}_{\boldsymbol{ij}}^{\boldsymbol{dist}} = 0\,, \tag{A6}$$

where $\boldsymbol{A}_{\boldsymbol{ij}}^{\boldsymbol{dist}} = 2 \cdot \begin{bmatrix} \hat{\hat{X}} - X_{0_{ij}} \\ \hat{\hat{Y}} - Y_{0_{ij}} \\ \hat{\hat{Z}} - Z_{0_{ij}} \end{bmatrix}^T$ and $\boldsymbol{B}_{\boldsymbol{ij}}^{\boldsymbol{dist}} = d_{ij}^2 + \hat{\hat{X}}^2 - X_{0_{ij}}^2 + \hat{\hat{Y}}^2 - Y_{0_{ij}}^2 + \hat{\hat{Z}}^2 - Z_{0_{ij}}^2$.

[2] The "double-hat" symbol "$\hat{\hat{\ }}$" indicates that a point close to $\boldsymbol{X}$ can be obtained through a rough estimate of the (final) estimate of $\boldsymbol{X}$ itself (i.e., $\hat{\boldsymbol{X}}$). We will illustrate how to determine $\hat{\hat{\boldsymbol{X}}}$ later.

A1.2 Angular sensors

From the local perspective of a generic (*ij*)-th angular sensor, two angles – i.e., θ_{ij} (azimuth) and φ_{ij} (elevation) – are subtended by the line passing through P and o_{ij} (see Figure A.2). Precisely, θ_{ij} describes the inclination of segment $o_{ij}P$ with respect to the plane $x_{ij}y_{ij}$ (with a positive sign when $z_{ij} > 0$), while φ_{ij} describes the counterclockwise rotation of the projection ($o_{ij}P'$) of $o_{ij}P$ on the $x_{ij}y_{ij}$ plane, with respect to the x_{ij} axis. Referring to the local coordinate system of the (*ij*)-th sensor, the following relationships hold:

$$\begin{aligned} &\theta_{ij} = \tan^{-1}\frac{y_{ij}}{x_{ij}} && \begin{cases} \text{if } x_{ij} \geq 0 \text{ then } -\frac{\pi}{2} \leq \theta_{ij} \leq \frac{\pi}{2} \\ \text{if } x_{ij} < 0 \text{ then } \frac{\pi}{2} < \theta_{ij} < \frac{3\pi}{2} \end{cases} \\ &\varphi_{ij} = \sin^{-1}\frac{z_{ij}}{o_{ij}P} && \left\{ -\frac{\pi}{2} \leq \varphi_{ij} \leq \frac{\pi}{2} \right. \end{aligned} \quad . \tag{A7}$$

Given that:

$$\tan\theta_{ij} = \frac{\sin\theta_{ij}}{\cos\theta_{ij}} \tag{A8}$$

and

$$o_{ij}P = \frac{o_{ij}P'}{\cos\varphi_{ij}} = \frac{x_{ij}/\cos\theta_{ij}}{\cos\varphi_{ij}} = \frac{x_{ij}}{\cos\theta_{ij}\cdot\cos\varphi_{ij}}, \tag{A9}$$

Eq. A7 can be reformulated as:

$$\begin{aligned} &x_{ij}\cdot\sin\theta_{ij} - y_{ij}\cdot\cos\theta_{ij} = 0 \\ &x_{ij}\cdot\sin\varphi_{ij} - z_{ij}\cdot\cos\theta_{ij}\cdot\cos\varphi_{ij} = 0 \end{aligned} . \tag{A10}$$

In matrix form, Eq. A10 becomes:

$$\boldsymbol{M_{ij}}\boldsymbol{x_{ij}} = \begin{bmatrix} \sin\theta_{ij} & -\cos\theta_{ij} & 0 \\ \sin\varphi_{ij} & 0 & -\cos\theta_{ij}\cdot\cos\varphi_{ij} \end{bmatrix} \cdot \begin{bmatrix} x_{ij} \\ y_{ij} \\ z_{ij} \end{bmatrix} = 0 \tag{A11}$$

The system of two equations in Eq. A11 can be expressed as a function of the global

coordinates of point *P*. Reversing Eq. A1, for switching from the local to the global coordinates, and considering that $\boldsymbol{R_{ij}}$ is orthonormal – therefore $\boldsymbol{R_{ij}^{-1}} = \boldsymbol{R_{ij}^{T}}$ (Hartley and Zisserman, 2003) – we obtain:

$$\boldsymbol{x_{ij}} = \boldsymbol{R_{ij}^{-1}}\left(\boldsymbol{X} - \boldsymbol{X_{0_{ij}}}\right) = \boldsymbol{R_{ij}^{T}}\left(\boldsymbol{X} - \boldsymbol{X_{0_{ij}}}\right). \tag{A12}$$

Combining Eqs. A11 and A12, we obtain:

$$\boldsymbol{M_{ij}}\boldsymbol{R_{ij}^{T}}\left(\boldsymbol{X} - \boldsymbol{X_{0_{ij}}}\right) = 0\,, \tag{A13}$$

from which:

$$\boldsymbol{M_{ij}}\boldsymbol{R_{ij}^{T}}\boldsymbol{X} - \boldsymbol{M_{ij}}\boldsymbol{R_{ij}^{T}}\boldsymbol{X_{0_{ij}}} = 0\,. \tag{A14}$$

We note that the equations of this system are linear with respect to the three (unknown) coordinates of *P*. Eq. A14 can be expressed in compact form, as:

$$\boldsymbol{A_{ij}^{ang}} \cdot \boldsymbol{X} - \boldsymbol{B_{ij}^{ang}} = 0\,, \tag{A15}$$

being $\boldsymbol{A_{ij}^{ang}} = \boldsymbol{M_{ij}}\boldsymbol{R_{ij}^{T}}$ and $\boldsymbol{B_{ij}^{ang}} = \boldsymbol{M_{ij}}\boldsymbol{R_{ij}^{T}}\boldsymbol{X_{0_{ij}}}$.

The matrix expression in Eq. A15 is similar to the one related to distance sensors (in Eq. A6). However, in the case of distance sensors, it encapsulates a single equation, while in the case of angular sensors, it encapsulates two equations.

A1.3 Note on hybrid sensors

A particular case is represented by *hybrid* sensors, which can be seen as special sensors integrating a distance sensor and an angular sensor (e.g., the sensors of a laser tracker/tracer). For these sensors, the usable equations for the localization problem are three: one related to a distance measurement ($\hat{d}_{ij}$) and two related to angular measurements ($\hat{\theta}_{ij}$, $\hat{\varphi}_{ij}$). These equations can be aggregated into a single linear system:

$$\boldsymbol{A_{ij}^{hyb}} \cdot \boldsymbol{X} - \boldsymbol{B_{ij}^{hyb}} = \begin{bmatrix} \boldsymbol{A_{ij}^{dist}} \\ \boldsymbol{A_{ij}^{ang}} \end{bmatrix} \cdot \boldsymbol{X} - \begin{bmatrix} \boldsymbol{B_{ij}^{dist}} \\ \boldsymbol{B_{ij}^{ang}} \end{bmatrix} = \boldsymbol{0}\,, \tag{A16}$$

where the superscript "*hyb*" stands for *hybrid* and $\boldsymbol{A}_{\boldsymbol{ij}}^{\boldsymbol{dist}}$, $\boldsymbol{B}_{\boldsymbol{ij}}^{\boldsymbol{dist}}$, $\boldsymbol{A}_{\boldsymbol{ij}}^{\boldsymbol{ang}}$ and $\boldsymbol{B}_{\boldsymbol{ij}}^{\boldsymbol{ang}}$ are the same matrices illustrated in Sects. A1.1 and A1.2.

The same system can be formulated in an alternative way. The (unknown) coordinates of *P*, with respect to the (same) local reference system related to the distance and the angular sensors, are given by (see Figure A.2):

$$\begin{cases} x_{ij} = d_{ij} \cdot \cos\varphi_{ij} \cdot \cos\theta_{ij} \\ y_{ij} = d_{ij} \cdot \cos\varphi_{ij} \cdot \sin\theta_{ij} \\ z_{ij} = d_{ij} \cdot \sin\varphi_{ij} \end{cases} . \tag{A17}$$

Combining Eqs. A1 and A17 we obtain:

$$\boldsymbol{R}_{\boldsymbol{ij}}^{T}\boldsymbol{X} - \boldsymbol{R}_{\boldsymbol{ij}}^{T}\boldsymbol{X}_{\boldsymbol{0}_{\boldsymbol{ij}}} = \left[d_{ij} \cdot \cos\varphi_{ij} \cdot \cos\theta_{ij} \quad d_{ij} \cdot \cos\varphi_{ij} \cdot \sin\theta_{ij} \quad d_{ij} \cdot \sin\varphi_{ij}\right]^{T} . \tag{A18}$$

We note that the equations of this system are linear with respect to the three (unknown) coordinates of *P* and can be expressed in compact form as:

$$\boldsymbol{A}_{\boldsymbol{ij}}^{\boldsymbol{hyb}} \cdot \boldsymbol{X} - \boldsymbol{B}_{\boldsymbol{ij}}^{\boldsymbol{hyb}} = 0 , \tag{A19}$$

where $\boldsymbol{A}_{\boldsymbol{ij}}^{\boldsymbol{hyb}} = \boldsymbol{R}_{\boldsymbol{ij}}^{T}$ and

$$\boldsymbol{B}_{\boldsymbol{ij}}^{\boldsymbol{hyb}} = \left[d_{ij} \cdot \cos\varphi_{ij} \cdot \cos\theta_{ij} \quad d_{ij} \cdot \cos\varphi_{ij} \cdot \sin\theta_{ij} \quad d_{ij} \cdot \sin\varphi_{ij}\right]^{T} + \boldsymbol{R}_{\boldsymbol{ij}}^{T}\boldsymbol{X}_{\boldsymbol{0}_{\boldsymbol{ij}}} .$$

The expression in Eq. A19 is certainly simpler and more compact than that in Eq. A16; however, it has a significant limitation: the three equations that it encapsulates (shown in Eq. A17) are coupled to each other, as they require the simultaneous knowledge of d_{ij}, θ_{ij} and φ_{ij}. For example, in the case d_{ij} only is available, while θ_{ij} and φ_{ij} not, none of the three equations can be used. For this reason, it seems more practical to use the formulation in Eq. A16[3], in which the distance and angular measurements are treated separately.

[3] Extending this reasoning, we also might find the way to decouple the equations relating to the angles (θ_{ij} and φ_{ij}) that are measured by angular sensors (see Eq. A7). However, this would unnecessarily complicate the formulation of the problem, without any practical reason: in fact, it is very unlikely that the same angular sensor provides a correct measurement for one angle and a wrong one for the other one.

A1.4 Weighting and solution

Considering a generic combination of LVM systems that are equipped with distance and/or angular sensors, the resulting linearized target-localization model is:

$$\boldsymbol{A}\cdot\boldsymbol{X}-\boldsymbol{B}=\begin{bmatrix}\boldsymbol{A}^{dist}\\ \boldsymbol{A}^{ang}\end{bmatrix}\cdot\boldsymbol{X}-\begin{bmatrix}\boldsymbol{B}^{dist}\\ \boldsymbol{B}^{ang}\end{bmatrix}=\boldsymbol{0}, \tag{A20}$$

where blocks $\boldsymbol{A}^{dist}$, $\boldsymbol{A}^{ang}$, $\boldsymbol{B}^{dist}$ and $\boldsymbol{B}^{ang}$ are defined as:

$$\boldsymbol{A}^{dist}=\begin{bmatrix}\vdots\\ \boldsymbol{A}_{ij}^{dist}\\ \vdots\end{bmatrix}_{ij\in I^{dist}},\ \boldsymbol{A}^{ang}=\begin{bmatrix}\vdots\\ \boldsymbol{A}_{ij}^{ang}\\ \vdots\end{bmatrix}_{ij\in I^{ang}},\ \boldsymbol{B}^{dist}=\begin{bmatrix}\vdots\\ \boldsymbol{B}_{ij}^{dist}\\ \vdots\end{bmatrix}_{ij\in I^{dist}},\ \boldsymbol{B}^{ang}=\begin{bmatrix}\vdots\\ \boldsymbol{B}_{ij}^{ang}\\ \vdots\end{bmatrix}_{ij\in I^{ang}},$$

where I^{dist} and I^{ang} are the sets of index-pair values (ij) relating to the distance and angular sensors respectively.

The system in Eq. 20 can be solved when at least three equations are available (e.g., P is seen by at least three distance sensors, or one distance sensor and one angular sensor, or two angular sensors, etc.). Since this system is generally overdefined (more equations than unknown parameters), there are several possible solution approaches, ranging from those based on the iterative minimization of a suitable error function (Franceschini et al., 2014) to those based on the Least Squares method (Wolberg, 2005).

It is worth remarking that the equations of the system may differently contribute to the uncertainty in the localization of P. Specifically, two of the main factors affecting this uncertainty are:

- *Uncertainty in the local measurements* ($\hat{d}_{ij}$, $\hat{\theta}_{ij}$ and $\hat{\varphi}_{ij}$), which generally depends on the metrological characteristics of sensors;
- *Relative position* between the point to be localized (P) and each (ij)-th sensor; e.g., assuming that the uncertainty in angular measurements is fixed, the uncertainty in the localization of P tends to increase proportionally to the *distance* between P and the angular sensors (Maisano and Mastrogiacomo, 2016);

- *Uncertainty in the position/orientation of sensors* ($\hat{X}_{0_{ij}}, \hat{Y}_{0_{ij}}, \hat{Z}_{0_{ij}}$, $\hat{\omega}_{ij}$, $\hat{\phi}_{ij}$ and $\hat{\kappa}_{ij}$), resulting from initial calibration process(es).

For simplicity, the proposed mathematical model considers only the first two factors, neglecting the third one (Maisano and Mastrogiacomo, 2016).

The sensors that mostly contribute to uncertainty in the localization of *P* are therefore the less accurate and/or the more distant from *P*.

Returning to the system in Eq. A20, it would be appropriate to solve it giving greater weight to the contributions from sensors that produce less uncertainty and *vice versa*. To this purpose, an elegant and practical method is that of the Generalized Least Squares (GLS) (Kariya and Kurata, 2004), in which a weight matrix ($\boldsymbol{W}$), which takes into account the uncertainty produced by the equations of the system. One of the most practical ways to define $\boldsymbol{W}$ is the application of the Multivariate Law of Propagation of Uncertainty to the system in Eq. A20, referring to the parameters affected by uncertainty (Hall, 2004). Assuming that such parameters are the distances or angles measured by each (*ij*)-th sensor, we collect them in a vector $\boldsymbol{\xi}$:

$$\boldsymbol{\xi} = \begin{bmatrix} \boldsymbol{\xi}^{dist} \\ \boldsymbol{\xi}^{ang} \end{bmatrix} = \begin{bmatrix} \begin{bmatrix} \vdots \\ d_{ij} \\ \vdots \end{bmatrix}_{ij \in I^{dist}} \\ \begin{bmatrix} \vdots \\ \begin{pmatrix} \theta_{ij} \\ \varphi_{ij} \end{pmatrix} \\ \vdots \end{bmatrix}_{ij \in I^{ang}} \end{bmatrix}. \tag{A22}$$

We remark that $\boldsymbol{\xi}$ is a vector containing the sensor local measurements, which can be decomposed in the two sub-vectors, $\boldsymbol{\xi}^{dist}$ and $\boldsymbol{\xi}^{ang}$, the former relating to distance sensors and the latter to angular sensors. For simplicity, we do not take into account the uncertainty related to the estimates of the location/orientation parameters of the sensors, which are contained in $\boldsymbol{X}_{\boldsymbol{0}_{ij}}$ and $\boldsymbol{R}_{ij}$ (Franceschini et al., 2011).

Propagating the uncertainty of the equations in Eq. A20 with respect to the elements in $\boldsymbol{\xi}$, we define $\boldsymbol{W}$ as:

$$\boldsymbol{W} = \left[\boldsymbol{J} \cdot \left(\boldsymbol{cov}(\boldsymbol{\xi})\right) \cdot \boldsymbol{J}^T\right]^{-1}. \tag{A23}$$

Let us now focus the attention on the elements in the second member of Eq. A23. $\boldsymbol{J}$ is the Jacobian (block-diagonal) matrix containing the partial derivatives of the elements in the first member of Eq. A20 with respect to the elements in $\boldsymbol{\xi}$:

$$\boldsymbol{J} = \begin{bmatrix} \boldsymbol{J^{dist}} & \boldsymbol{0} \\ \boldsymbol{0} & \boldsymbol{J^{ang}} \end{bmatrix} = \begin{bmatrix} \begin{bmatrix} \ddots & & \boldsymbol{0} \\ & \boldsymbol{J_{ij}^{dist}} & \\ \boldsymbol{0} & & \ddots \end{bmatrix}_{ij \in I^{dist}} & \boldsymbol{0} \\ \boldsymbol{0} & \begin{bmatrix} \ddots & & \boldsymbol{0} \\ & \boldsymbol{J_{ij}^{ang}} & \\ \boldsymbol{0} & & \ddots \end{bmatrix}_{ij \in I^{ang}} \end{bmatrix}, \tag{A24}$$

where blocks $\boldsymbol{J_{ij}^{dist}}$ and $\boldsymbol{J_{ij}^{ang}}$ are defined as

$$\begin{aligned} \boldsymbol{J_{ij}^{dist}} &= \begin{bmatrix} 2 \cdot d_{ij} \end{bmatrix} \\ \boldsymbol{J_{ij}^{ang}} &= \begin{bmatrix} x_{ij} \cdot \cos\theta_{ij} + y_{ij} \cdot \sin\theta_{ij} & 0 \\ z_{ij} \cdot \sin\theta_{ij} \cdot \cos\varphi_{ij} & x_{ij}\cos\varphi_{ij} + z_{ij} \cdot \cos\theta_{ij} \cdot \sin\varphi_{ij} \end{bmatrix}, \end{aligned} \tag{A25}$$

and the remaining elements of the matrix are all zeros.

Returning to the description of Eq. A22, $\boldsymbol{cov(\xi)}$ is the covariance matrix of $\boldsymbol{\xi}$, defined as:

$$\boldsymbol{cov}(\boldsymbol{\xi}) = \begin{bmatrix} \boldsymbol{cov}\left(\boldsymbol{\xi^{dist}}\right) & \boldsymbol{0} \\ \boldsymbol{0} & \boldsymbol{cov}\left(\boldsymbol{\xi^{ang}}\right) \end{bmatrix} = \begin{bmatrix} \begin{bmatrix} \ddots & & \boldsymbol{0} \\ & \boldsymbol{cov}\left(\boldsymbol{\xi_{ij}^{dist}}\right) & \\ \boldsymbol{0} & & \ddots \end{bmatrix}_{ij \in I^{dist}} & \boldsymbol{0} \\ \boldsymbol{0} & \begin{bmatrix} \ddots & & \boldsymbol{0} \\ & \boldsymbol{cov}\left(\boldsymbol{\xi_{ij}^{ang}}\right) & \\ \boldsymbol{0} & & \ddots \end{bmatrix}_{ij \in I^{ang}} \end{bmatrix}, \tag{A26}$$

where blocks $\boldsymbol{cov}\left(\boldsymbol{\xi_{ij}^{dist}}\right)$ and $\boldsymbol{cov}\left(\boldsymbol{\xi_{ij}^{ang}}\right)$ are defined as

$$\boldsymbol{cov}\left(\boldsymbol{\xi}_{\boldsymbol{ij}}^{\boldsymbol{dist}}\right)=\left[\sigma_{d_{ij}}^{2}\right]$$
$$\boldsymbol{cov}\left(\boldsymbol{\xi}_{\boldsymbol{ij}}^{\boldsymbol{ang}}\right)=\begin{bmatrix}\sigma_{\theta_{ij}}^{2} & 0\\ 0 & \sigma_{\varphi_{ij}}^{2}\end{bmatrix}. \qquad \text{(A27)}$$

We notice that the diagonal elements of $\boldsymbol{cov}(\boldsymbol{\xi})$ are the variances related to the distances and angles measured by the individual sensors (Sect. 3.1.1 illustrates some practical ways to estimate these parameters). The off-diagonal entries of these blocks are zeros, assuming no correlation between the local measurements by a generic sensor; the off-block-diagonal entries are zeros, assuming that sensors work independently from each other and there is no correlation between the local measurements related to different sensors.

By applying the GLS method to the system in Eq. A20, we obtain the final position estimate of *P* as:

$$\hat{\boldsymbol{X}}=\left(\boldsymbol{A}^{T}\cdot\boldsymbol{W}\cdot\boldsymbol{A}\right)^{-1}\cdot\boldsymbol{A}^{T}\cdot\boldsymbol{W}\cdot\boldsymbol{B}\,. \qquad \text{(A28)}$$

For further details on the GLS method, see (Kariya and Kurata, 2004).

We emphasize that an (at least rough) initial estimate of $\boldsymbol{X}$ is required to define some elements of the blocks $\boldsymbol{A}_{\boldsymbol{ij}}^{\boldsymbol{dist}}$ (see Eq. A6) and $\boldsymbol{J}_{\boldsymbol{ij}}^{\boldsymbol{ang}}$ (see Eq. A25). This problem can be overcome applying the formula in Eq. A28 recursively: (i) setting no-matter-what initial $\hat{\hat{\boldsymbol{X}}}$, in order to determine the elements of blocks $\boldsymbol{A}_{\boldsymbol{ij}}^{\boldsymbol{dist}}$ and $\boldsymbol{J}_{\boldsymbol{ij}}^{\boldsymbol{ang}}$, (ii) obtaining a not very accurate localization of *P*, and (iii) iterating the localization using the result of the previous one as a new $\hat{\hat{\boldsymbol{X}}}$. We verified that the localization tends to converge to the correct solution after no more than five-ten iterations.